Nuclear Science and Techniques (2025) 36:182
https://doi.org/10.1007/s41365-025-01752-x

Intrinsic detection efficiency and true coincidence summing correction for a low-background γ spectrometer with a well-type HPGe detector

Ming-Hao Zhu[1] · You-Bao Wang[1] · Qiang Wang[1] · Yu-Qiang Zhang[1] · Jin-Long Ma[1] · Zhi-Wei Qin[2] · Jun Su[2] · Fu-Qiang Cao[1] · Zhi-Cheng Zhang[1] · Yu-Wen Chen[1] · Jiang-Lin Hou[1] · Chang-Xin Guo[1] · Sheng-Quan Yan[1] · Yun-Ju Li[1] · Yang-Ping Shen[1] · Bing Guo[1,3] · Wei-Ping Liu[1,4]

Received: 25 December 2024 / Revised: 28 January 2025 / Accepted: 16 February 2025 / Published online: 17 July 2025

Abstract
A low-background γ spectrometer named the Gamma spectrometer for Nuclear Activation Studies (GNAS) was developed to detect scarce γ radioactivity, with a special focus on conducting activation experiments in nuclear astrophysics. It consisted of a well-type HPGe detector surrounded by optimized multi-layer shielding, which reduced the laboratory background counting rate by 99.5% and enabled a sensitivity edge as low as 0.044 Bq for the 477.6 KeV γ line of ^{7}Be. The near 4π geometry of the HPGe detector introduces a severe true coincidence summing (TCS) effect along with its high detection efficiency. To determine the intrinsic detection efficiency and correct for the TCS effect, a Monte Carlo simulation method was developed with the Geant4 toolkit. The detector model was optimized by matching the simulated full energy peak (FEP) statistics with those of a ^{137}Cs monoenergetic source and calibrated ^{55,57,58}Co sources produced by low-energy proton beam bombardment of natural iron. The intrinsic detection efficiency curve was obtained, and an algorithm for the correction of the TCS effect was programmed using decay data from the ENSDF library and Nuclear Wallet Cards. The GNAS fulfills the requirements of the ongoing activation measurement of proton- and alpha-induced reactions in nuclear astrophysics on the ground and at the Jinping Underground Nuclear Astrophysics (JUNA) facility.

Keywords Low-background γ spectrometer · GNAS · Well-type HPGe detector · True coincidence summing · Activation measurement at JUNA

1 Introduction

Nuclear reactions play a significant role in energy generation and the synthesis of elements in the universe [1]. H, He, and a small amount of Li were produced by primordial nucleosynthesis in the first few minutes after the Big Bang [2–4]. During the stellar burning phases, elements up to Fe are produced by a series of charged-particle-induced nuclear reactions [5, 6], and their reaction rates are commonly hindered by the small Coulomb barrier tunneling probability at astrophysical energies, which makes direct measurements at the Gamow window extremely challenging [7–10]. The activation method is an alternative approach to measure the cross section by irradiating the target and determining the number of reaction product nuclei separately [11]. It involves the use of an accelerator mass spectrometer [12] for direct counting or a low-background γ spectrometer for the decay γ-rays with a known branching ratio [13]. If the reaction product nuclei

This work was supported by the National Key Research and Development Project (No. 2022YFA1602301), the National Natural Science Foundation of China (Nos. U2267205 and 12275361), and the Continuous-Support Basic Scientific Research Project.

✉ You-Bao Wang
ybwang@ciae.ac.cn

[1] Department of Nuclear Physics, China Institute of Atomic Energy, Beijing 102413, China

[2] Key Laboratory of Beam Technology of Ministry of Education, School of Physics and Astronomy, Beijing Normal University, Beijing 100875, China

[3] School of Physics, Xi'an 710049, China

[4] College of Science, Southern University of Science and Technology, Shenzhen 518055, China

are radioactive and have a suitable half-life, the activation method with offline decay γ-ray detection provides a portable solution to avoid the difficulties encountered in online direct measurement.

A γ spectrometer with high detection efficiency and low background is essential for this purpose. A low background can be achieved by active and passive shielding of cosmic and laboratory γ-rays [14, 15]. A well-type HPGe detector has an almost 4π geometry when placing the radioactive sample in the well bottom, thus making it ideal for achieving high detection efficiency and energy resolution simultaneously [16, 17]. This is vital for the upcoming astrophysical reaction measurements of ^{3}He$(\alpha,\gamma)^{7}$Be, etc. [18], at Jinping Underground Nuclear Astrophysics (JUNA) [19–24] via the activation method. However, the near 4π geometry of a well-type HPGe detector introduces a severe true coincidence summing (TCS) effect from cascade γ-rays [25, 26]; therefore, the measured γ spectrum must be deconvoluted for true full energy peak (FEP) statistics and intrinsic efficiency.

In this study, a low-background γ spectrometer called the Gamma spectrometer for Nuclear Activation Study (GNAS) was developed with a well-type HPGe detector and optimized multi-layer shielding with elaborately selected materials. A Monte Carlo simulation approach was applied to retrieve the intrinsic detection efficiency and correct for the TCS effect with a ^{137}Cs monoenergetic source and online-produced ^{55,57,58}Co sources. By simulating the HPGe detector response and comparing the simulated decay spectra with those measured from irradiated natural Fe samples, the intrinsic detection efficiency of the GNAS was obtained. An algorithm for the correction of the TCS effect was programmed using decay data from the ENSDF library and Nuclear Wallet Cards.

2 GNAS description

The GNAS is based on an ORTEC GWL series HPGe well-type detector with a low-background oxygen-free copper endcap and a high-purity aluminum well tube. The active volume of the germanium detector is 349 cm^3, with a well 1.55 cm in diameter and 4.0 cm in depth. The detector is equipped with a low-background J-type cryostat and a remote preamplifier. Because it is near the 4π geometry for small radioactive samples, the detector has a high absolute counting efficiency for radiochemical analysis and low-level γ-ray spectroscopy.

Figure 1 shows the energy resolution curve of the detector, defined as the ratio of the FWHM to γ energy, which was measured using a mixed γ radioactive source of ^{152}Eu and ^{133}Ba. The FWHM of the GNAS at 1408 keV was 2.33 keV, which is similar to that of other coaxial p-type HPGe detectors.

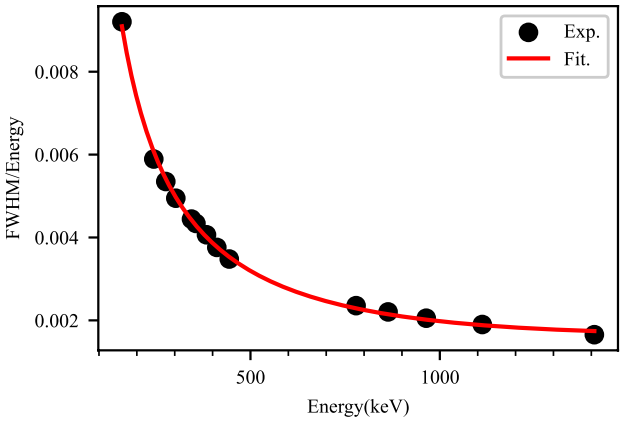

Fig. 1 (Color online) Energy resolution curve of the GNAS. The solid circles represent the experimental measurement, whereas the line is the fitting curve with a formula of $1.43/E + 4.35 \times 10^{-7} \cdot E + 0.000113$ (E in keV)

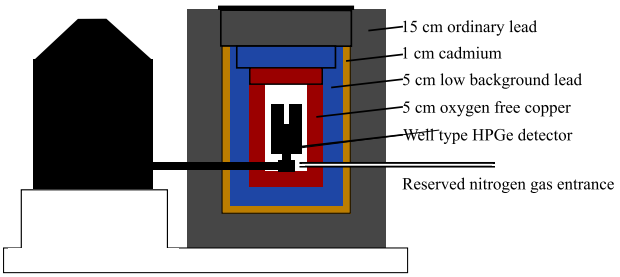

Fig. 2 (Color online) Schematic of the low-background γ spectrometer GNAS (not to scale)

A schematic of the low-background γ spectrometer GNAS is shown in Fig. 2. The germanium detector is set in a chamber with a diameter of 12 cm and a height of 41 cm surrounded by 5cm-thick high-purity oxygen-free copper. The copper layer is then enclosed by 5cm-thick low-background lead, 1cm-thick cadmium, and 15cm-thick ordinary lead. The cadmium layer is used to absorb the thermalized background neutrons [27]. The inner layer of the low-background lead and oxygen-free copper is used to shield the outside and secondary γ radiation from neutron absorption, respectively.

The background γ counting rate spectra with and without shielding are shown in Fig. 3. With the multi-layer shielding structure of the GNAS, its background counting rate in the energy range 195–2910 keV decreased from 185.74 counts per second (cps) to 0.89 cps, a reduction rate of approximately 99.5%.

To measure offline the decay γ-rays from nuclear activation experiments, the energy range of interest for γ-rays typically does not exceed 3 MeV. In this energy range, the background γ spectrum is highly complex, as shown in Fig. 3. These γ-rays mainly originate from environmental

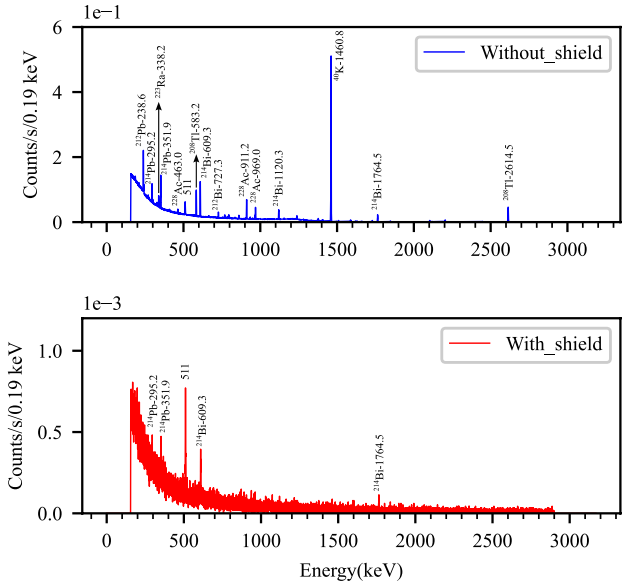

Fig. 3 (Color online) GNAS background γ spectra with and without shielding

radioactivity, including the natural radioactive series of ^{238}U and ^{232}Th, the single radionuclide ^{40}K, and the background neutron-induced series [28]. With the multi-layer shielding structure of the GNAS, most background γ lines were reduced to an unnoticeable level. The γ lines at 295.2 keV and 351.9 keV arose from ^{214}Pb, whereas those at 609.3 keV and 1764.5 keV arose from ^{214}Bi, which originated from shielding materials and radon in the air [28–30]. The γ line at 511 keV originated from the annihilation of positrons produced mainly by the high-energy environmental γ-ray-induced pair production in the germanium crystal.

The peak counting rates of the background γ lines of ^{214}Pb and ^{214}Bi with and without the shielding are listed in Table 1.

It is planned that the GNAS will be used at JUNA for activation experiments; therefore, it will be necessary to introduce nitrogen gas into the HPGe detector room to remove the natural radon background.

Table 1 Peak counting rate of the background γ lines of ^{214}Pb and ^{214}Bi in the GNAS

Energy (keV)	Nuclide	Peak counting rate (Day^{-1})	
		With shield	Without shield
295.2	^{214}Pb	<137	40543(898)
351.9	^{214}Pb	178(16)	74423(845)
511	β^+	1010(54)	44137(759)
609.3	^{214}Bi	131(13)	83575(668)
1120.3	^{214}Bi	<86	26673(469)
1764.5	^{214}Bi	<36	25071(268)

The significant decrease in the background and the blind well design of HPGe enhanced the sensitivity of the GNAS. Several low-activity ^{7}Be samples were prepared using the ^{7}Li(p, n)^{7}Be reaction. The decay spectra of ^{7}Be with different activities are shown in Fig. 4.

The counting rate of 477.6 keV γ-rays is 199(39) counts per day (cpd) in Fig. 4a and 94(47) cpd in Fig. 4b. For a sample with an activity as low as 0.044 Bq, which is less than 4.5×10^{-3} s^{-1} out of the emission rate of 477.6 keV γ rays, the GNAS was still capable of distinguishing and evaluating its statistics, as shown in Fig. 4b.

3 True coincidence summing

The intrinsic FEP efficiency of a γ spectrometer is typically calculated using Eq. (1) and standard γ sources with known activities and γ branching ratios,

$$\varepsilon(E) = \frac{\lambda N(E)}{A(E) \cdot \eta(E) \cdot \left(1 - \mathrm{e}^{-\lambda t}\right)}, \tag{1}$$

where E is the energy of the decay γ, $N(E)$ is the net area of the FEP, $A(E)$ is the activity of the source at the start of

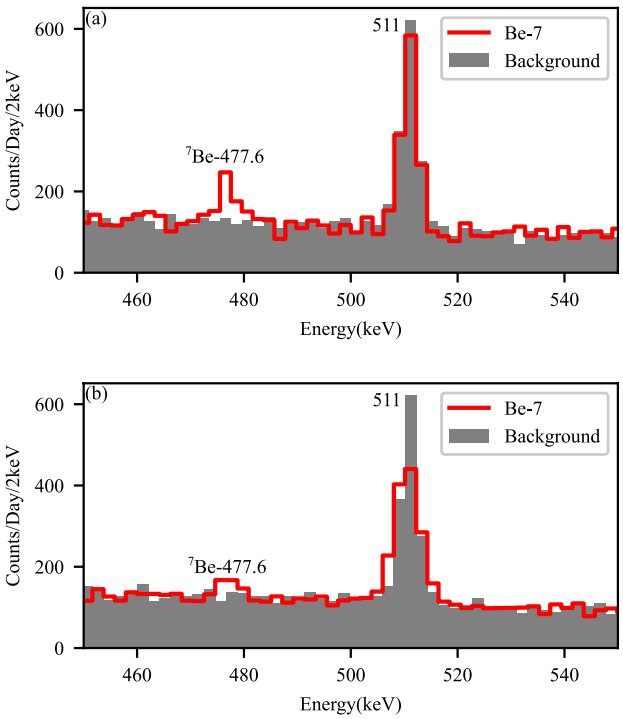

Fig. 4 (Color online) γ spectra from the decay of ^{7}Be samples with different activities, 0.074 Bq in (**a**), and 0.044 Bq in (**b**). As an example of nuclear activation study, the ^{7}Be activity was determined via GNAS measurement, as shown in (**a**), and via decay law evaluation, as shown in (**b**), when the remeasurement was performed

the measurement, $\eta(E)$ is the branching ratio, λ is the decay constant, and t is the measurement time. Such a measurement should take place with the sources separated 20~30 cm from the detector, which inevitably results in a low detection efficiency if a HPGe detector is used. However, the GNAS has high efficiency from the near 4π geometry; therefore, the TCS effect must be well resolved. When two or more γ -rays deposit their energies within the resolving time of the HPGe detector, the detector records them as one γ line with summed energy [26, 31]. This effect is particularly significant for cascade γ-rays emitted sequentially from the same nucleus. When TCS occurs, the FEP statistics are shifted, and the correction of TCS depends on the decay scheme of the individual radioactive nuclei. Even the γ spectra of most standard sources need to be deconvolved; therefore, an algorithm must be developed to determine the intrinsic detection efficiency of the GNAS and the correction for TCS.

For two cascade γ-rays, there are three types of TCS: (1) both γ-rays deposit their full energies in the active volume of the HPGe detector; (2) one γ-ray deposits its full energy, whereas the other deposits only part of its energy; and (3) both γ-rays deposit only part of their energies. The first two types of summing events can significantly deflect the FEP statistics in the γ spectrum, which is represented by $N(E)$ in Eq. (1). The third type of summing event contributes only to the Compton plateau in the spectrum, which is not directly attributed to the statistics of the FEPs.

3.1 Correction for TCS

Numerical methods have been developed to correct for TCS effects in γ-ray spectroscopy [32–35]. In recent years, Monte Carlo simulations have been intensively used to determine the detection efficiency and TCS correction of various customized γ spectrometers [36–39]. The ideal method for determining the intrinsic FEP efficiency of the GNAS is through a set of weak monoenergetic γ-ray sources [40–42], which in turn helps to determine the dimensional parameters of the HPGe detector for the simulation. For this purpose, a right-sized ^{137}Cs source with an activity of only 601 Bq was fabricated. Because we did not have other weak monoenergetic γ-ray sources, several natural Fe targets were irradiated using a 4 MeV proton beam from the HI-13 tandem accelerator, and the activities of ^{55}Co, ^{57}Co, and ^{58}Co were subsequently calibrated using a standard γ spectrometer [43]. Based on these γ sources, we developed a Monte Carlo simulation method using the Geant4 toolkit.

The primary task of the simulation was to determine the dimensional parameters of the well-type HPGe detector, with which the intrinsic FEP efficiency $\varepsilon_{\mathrm{inc}}$ could be directly simulated at the user-set γ-ray energies. The next step was to simulate real radioactive decay to correct the TCS effect numerically.

With Geant4, decay data can be generated from the G4RadioactiveDecayPhysics module based on the ENSDF library and Nuclear Wallet Cards. The G4EmLowEPPhysics package is used to describe low-energy polarized X/γ -ray transport [44]. A ^{55}Co decay event at the bottom of the well and its interactions with the germanium crystal are schematically shown in Fig. 5. The emitted positron annihilated into two 511 keV γ-rays, whereas the ^{55}Fe daughter nucleus deexcited by single or cascaded γ lines. The energy deposited in the detector by each decay was treated as a single signal; therefore, these γ-rays may partly or totally sum into a single γ line.

The HPGe dimensions provided by the manufacturer were optimized [40, 45] to reproduce the known activities of the ^{55,57,58}Co spectrum, as listed in Table 2.

The dead layer and well tube thicknesses were found to significantly affect the efficiency in the low-energy region because of the absorption of γ lines. The dimensions of the crystals also affected the efficiency, owing to the solid angle and crystal thickness difference.

The dead layer and well tube thicknesses were preliminarily optimized to constrain the deviation between the simulated and experimental ^{137}Cs statistics to within 10%. Subsequently, most parameters were varied in small steps and eventually constrained by the experimental spectra of the ^{55,57,58}Co source to obtain the optimized values. For example, the simulated γ spectrum containing the calibrated ^{55,57,58}Co activities was compared with the measured spectrum, as shown in Fig. 6. All FEPs and summing peaks were accurately reproduced in the simulation. For instance, the 1321.76 keV and 1832.76 keV γ-ray peaks,

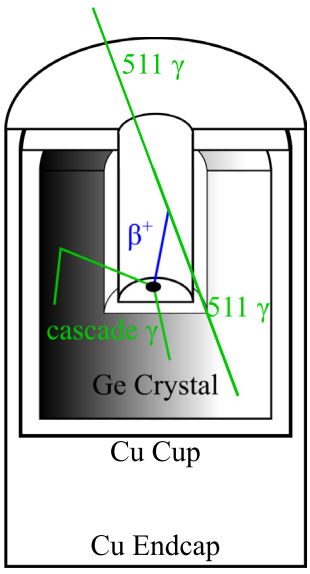

Fig. 5 (Color online) Schematic description of a ^{55}Co decay event and its interactions with the germanium crystal (shielding layers are hidden; not to scale)

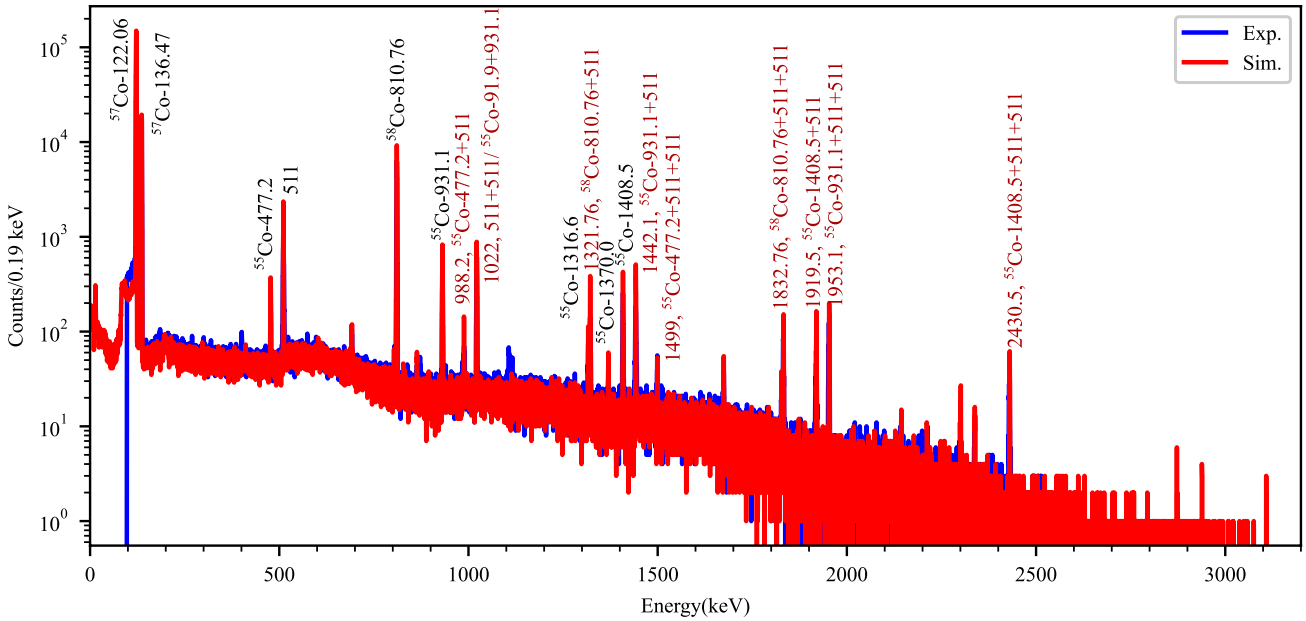

Fig. 6 (Color online) Simulated and measured spectra of an irradiated sample containing calibrated ^{55}Co, ^{57}Co, and ^{58}Co activities. Peaks from TCS are marked in red. All the FEPs and summing peaks are well reproduced in the simulation

Table 2 Manufacturer-provided and optimized HPGe dimensions

Detector parameters	Manufacturer	Optimized
Crystal diameter	79.3 mm	79.3 mm
Crystal length	77 mm	79.5 mm
Dead layer thickness	0.3 μm	0.6 μm
Endcap thickness	-	0.8 mm
Endcap-to-crystal distance	-	10.3 mm
Well tube thickness	1 mm	0.65 mm
Well tube inner diameter	15.5 mm	15.5 mm
Well tube active depth	40 mm	40 mm
Coaxial hole diameter	-	33.34 mm
Coaxial hole depth	-	50 mm

which were the summing peaks of 810.76 keV and one or two 511 keV γ-rays from ^{58}Co, were well reproduced.

To evaluate the simulation uncertainty of the detector parameter optimization, the ratios of the simulated and experimental γ FEP areas for the ^{137}Cs and ^{55,57,58}Co sources are shown in Fig. 7. Most of the simulated FEP areas agreed with the experimental areas within a 5% margin of error. The γ lines with large deviations were mainly due to weak activities and uncertainties in the calibrated activity value. To reduce the uncertainty, a ^{65}Zn ($t_{1/2}$ = 244.26 d) source with near 1115.6 keV monoenergetic γ radioactivity will be produced at the HI-13 tandem accelerator using the ^{65}Cu(p, n) ^{65}Zn reaction.

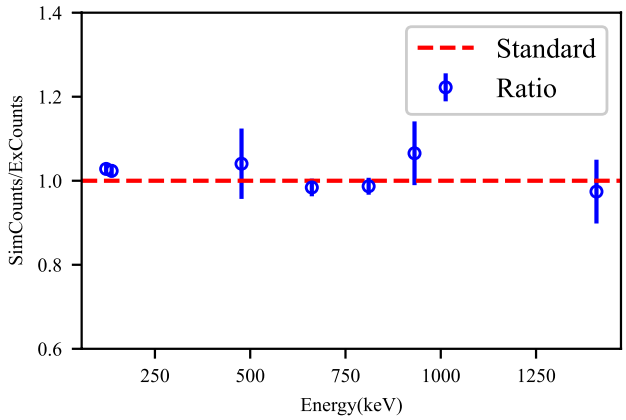

Fig. 7 (Color online) Ratio of the simulated and experimental γ FEP areas for the ^{137}Cs and ^{55,57,58}Co sources. The error bars are from the uncertainties of the relevant γ-ray FEP statistics and calibrated activity value

3.2 Intrinsic efficiency and TCS correction factor

Using the optimized detector model, we calculated the intrinsic FEP efficiency of the GNAS using different energy steps of Geant4 simulations. The resulting efficiency curve is presented in Fig. 8. To illustrate the impact of TCS, the specific energy points from ^{137}Cs and ^{55,57,58}Co are marked. These points represent the efficiencies obtained directly from the measured FEP statistics

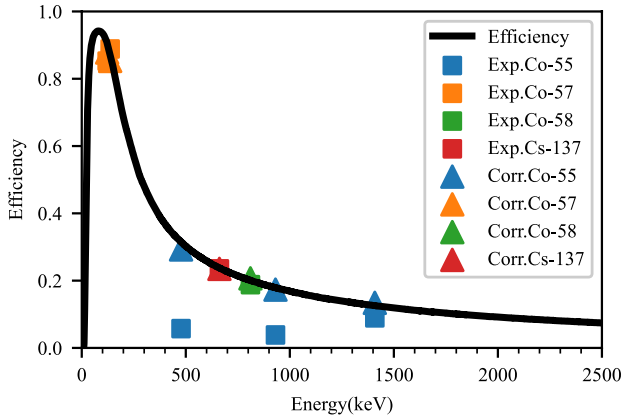

Fig. 8 (Color online) Intrinsic efficiency curve of the GNAS. Several energy points from ^{137}Cs and ^{55,57,58}Co with and without correction for TCS are marked. ^{57}Co can be regarded as a quasi-monoenergetic source without a γ cascade and 511 keV γ-rays from β^+ decay, whereas ^{55}Co suffers heavy TCS owing to significant cascade γ-rays

Table 3 Measured (ε_{exp}) and simulated (ε_{sim}) uncorrected FEP efficiencies, TCS correction factor (F_{TCS}), and FEP efficiencies (ε_{inc}) after TCS corrections

Nuclide	E_γ (keV)	ε_{exp}	ε_{sim}	F_{TCS}	ε_{inc}
^{137}Cs	661.6	0.235(1)	0.235(1)	1	0.235(1)
^{55}Co	477.2	0.057(3)	0.061(6)	5.1(5)	0.3153(6)
	931.1	0.039(2)	0.039(4)	4.5(5)	0.1788(4)
	1408.5	0.089(5)	0.083(8)	1.5(1)	0.1260(4)
^{57}Co	122.1	0.852(10)	0.879(16)	1.03(2)	0.9063(10)
	136.5	0.889(11)	0.913(17)	0.96(2)	0.8745(9)
^{58}Co	810.8	0.188(3)	0.182(5)	1.10(3)	0.2007(4)

according to Eq. 1 with and without correction for the TCS effect.

If we define a TCS correction factor as the ratio of the intrinsic FEP efficiency ε_{inc} to that without correcting for TCS ε_{nc},

$$F_{TCS} = \frac{\varepsilon_{inc}}{\varepsilon_{nc}}, \tag{2}$$

where ε_{inc} can be simulated using the user-set γ-ray energy, and ε_{nc} can be calculated from the simulation spectra, such as that shown in Fig. 6.

Detailed data are presented in Table 3, which lists the measured and simulated uncorrected FEP efficiencies as well as the TCS correction factor and intrinsic FEP efficiencies after TCS corrections. For certain γ-ray peaks, such as the 477.2 keV and 931.1 keV lines from ^{55}Co, the TCS effect was particularly pronounced because of the cascade γ decay and high efficiency of the detector.

For activation measurements in nuclear astrophysics at JUNA, when the produced radioactive nuclei decay through cascade γ-rays, TCS evidently deflects the real FEP statistics. With the newly developed Monte Carlo method, one can simulate the TCS correction factor by simply changing the decay nucleus together with the well-determined intrinsic detection efficiency curve of the GNAS.

4 Summary

A low-background γ spectrometer (GNAS) was installed for activation measurements within nuclear astrophysics. Using a multi-layer shielding structure, a background reduction of 99.5% was achieved, which enabled the detection edge of a low activity of 10^{-2} Bq with a high-efficiency well-type HPGe. A Monte Carlo simulation approach using Geant4 was developed to address the TCS effect. The optimized detector model ensured a good agreement between the simulated and experimental spectra. The intrinsic efficiency curve was determined, and the algorithm for TCS correction was programed using decay data from the ENSDF library and Nuclear Wallet Cards. The GNAS fulfills the requirements of the ongoing activation measurement of proton- and alpha-induced reactions in nuclear astrophysics on the ground and at the JUNA facility.

Author contributions All authors contributed to the study conception and design. You-Bao Wang, Jun Su and Ming-Hao Zhu contributed to the conceptualization and methodology. Material preparation, data collection and analysis were performed by Ming-Hao Zhu, You-Bao Wang, Qiang Wang, Yu-Qiang Zhang, Jin-Long Ma, Zhi-Wei Qin, Jun Su, Fu-Qiang Cao, Zhi-Cheng Zhang, Yu-Wen Chen, Jiang-Lin Hou, Chang-Xin Guo, Sheng-Quan Yan, Yun-Ju Li, Yang-Ping Shen, Bing Guo, and Wei-Ping Liu. The first draft of the manuscript was written by Ming-Hao Zhu, and all authors commented on previous versions of the manuscript. All authors read and approved the final manuscript.

Data availability The data that support the findings of this study are openly available in Science Data Bank at https://cstr.cn/31253.11.sciencedb.j00186.00695 and https://www.doi.org/10.57760/sciencedb.j00186.00695.

Declarations

Conflict of interest The authors declare that they have no conflict of interests.

References

1. E.M. Burbidge, G.R. Burbidge, W.A. Fowler et al., Synthesis of the elements in stars. Rev. Mod. Phys. **29**, 547–650 (1957). https://doi.org/10.1103/RevModPhys.29.547

2. J. Hou, N. Prantzos, Galactic abundance gradients and implications for nucleosynthesis. Nucl. Phys. A **688**, 411–413 (2001). https://doi.org/10.1016/S0375-9474(01)00740-0
3. H. Reeves, On the origin of the light elements (Z<6). Rev. Mod. Phys. **66**, 193–216 (1994). https://doi.org/10.1103/RevModPhys.66.193
4. R.H. Cyburt, B.D. Fields, K.A. Olive et al., Big bang nucleosynthesis: present status. Rev. Mod. Phys. **88**, 015004 (2016). https://doi.org/10.1103/RevModPhys.88.015004
5. W.P. Liu, Z.H. Li, X.X. Bai et al., Measurements of stellar and explosive nuclear astrophysics reactions. Chin. Phys. C **32**, 59–63 (2008). https://hepnp.ihep.ac.cn/en/article/id/a7e5fdb2-261e-4325-a286-93b2f1fcac90
6. D.D. Clayton, S.E. Woosley, Thermonuclear astrophysics. Rev. Mod. Phys. **46**, 755–771 (1974). https://doi.org/10.1103/RevModPhys.46.755
7. C. Bruno, Experimental challenges in low-energy nuclear astrophysics. J. Phys: Conf. Ser. **1078**, 012007 (2018). https://doi.org/10.1088/1742-6596/1078/1/012007
8. W.K. Nan, Y.B. Wang, Y.D. Sheng et al., Novel thick-target inverse kinematics method for the astrophysical $^{12}C + ^{12}C$ fusion reaction. Nucl. Sci. Tech. **35**, 208 (2024). https://doi.org/10.1007/s41365-024-01573-4
9. Y.J. Chen, H. Zhang, L.Y. Zhang et al., Direct measurement of the break-out $^{19}F(p,\gamma)^{20}Ne$ reaction in the China Jinping underground laboratory (CJPL). Nucl. Sci. Tech. **35**, 143 (2024). https://doi.org/10.1007/s41365-024-01531-0
10. L. Zhang, J. He, R.J. deBoer et al., Measurement of $^{19}F(p,\gamma)^{20}Ne$ reaction suggests CNO breakout in first stars. Nature **610**, 656–660 (2022). https://doi.org/10.1038/s41586-022-05230-x
11. G. Gyürky, Z. Fülöp, F. Käppeler et al., The activation method for cross section measurements in nuclear astrophysics. Eur. Phys. J. A **55**, 41 (2019). https://doi.org/10.1140/epja/i2019-12708-4
12. Y. Zhang, S.Q. Yan, M. He et al., Stepped-up development of accelerator mass spectrometry method for the detection of ^{60}Fe with the HI-13 tandem accelerator. Nucl. Sci. Tech. **35**, 77 (2024). https://doi.org/10.1007/s41365-024-01453-x
13. I. Dillmann, L. Coquard, C. Domingo-Pardo et al., Cross sections for proton-induced reactions on Pd isotopes at energies relevant for the γ process. Phys. Rev. C **84**, 015802 (2011). https://doi.org/10.1103/PhysRevC.84.015802
14. Q. Hu, H. Ma, J. He et al., Design of cosmic veto shielding for HPGe-detector spectrometer. Appl. Radiat. Isotopes **109**, 474–478 (2016). Proceedings of the 20th International Conference on Radionuclide Metrology and its Applications 8–11 June 2015, Vienna, Austria. https://doi.org/10.1016/j.apradiso.2015.11.065
15. I. Radulescu, A. Blebea-Apostu, R. Margineanu et al., Background radiation reduction for a high-resolution gamma-ray spectrometer used for environmental radioactivity measurements. Nucl. Instrum. Methods Phys. Res. Sect. A **715**, 112–118 (2013). https://doi.org/10.1016/j.nima.2013.03.024
16. G.C. Yang, L.M. Hua, F. Lu et al., Response functions of a 4π summing gamma detector in β-oslo method. Nucl. Sci. Tech. **33**, 68 (2022). https://doi.org/10.1007/s41365-022-01058-2
17. C.G. Yan, Improvement of accuracy of efficiency extrapolation method in $4\pi\beta - \gamma$ coincidence counting. Nucl. Instrum. Methods Phys. Res. Sect. A **369**, 383–387 (1996). https://doi.org/10.1016/S0168-9002(96)80014-3
18. Y. Li, Z. Li, Y. Wang et al., The controversy 3/2+ state in ^{7}Be and its effect on the $^{3}He(\alpha,\gamma)^{7}Be$ reaction. Nucl. Phys. A **1022**, 122444 (2022). https://doi.org/10.1016/j.nuclphysa.2022.122444
19. W.P. Liu, B. Guo, Z. An et al., Recent progress in nuclear astrophysics research and its astrophysical implications at the china institute of atomic energy. Nucl. Sci. Tech. **35**, 217 (2024). https://doi.org/10.1007/s41365-024-01590-3
20. W.P. Liu, J. collaboration), First results from the underground nuclear reaction experiments in JUNA. Chin. Phys. Lett. **40**, 060401 (2023). https://doi.org/10.1088/0256-307X/40/6/060401
21. T. Kajino, Underground laboratory JUNA shedding light on stellar nucleosynthesis. Nucl. Sci. Tech. **34**, 42 (2023). https://doi.org/10.1007/s41365-023-01196-1
22. W.P. Liu, Z.H. Li, J.J. He et al., Progress of underground nuclear astrophysics experiment JUNA in china. Few-Body Syst. **63**, 43 (2022). https://doi.org/10.1007/s00601-022-01735-3
23. C. Chen, Y.J. Li, H. Zhang et al., Preparation of large-area isotopic magnesium targets for the $^{25}Mg(p,\gamma)^{26}Al$ experiment at JUNA. Nucl. Sci. Tech. **31**, 91 (2020). https://doi.org/10.1007/s41365-020-00800-y
24. L. Zhang, J. He, R.J. deBoer et al., Progress of Jinping underground laboratory for nuclear astrophysics (JUNA). Sci. China Phys. Mech. Astron. **59**, 642001 (2016). https://doi.org/10.1007/s11433-016-5785-9
25. C. Zhong, Empirical relation between efficiency and volume of HPGe detectors. Nucl. Instrum. Methods Phys. Res. Sect. A **262**, 439–440 (1987). https://doi.org/10.1016/0168-9002(87)90885-0
26. K. Debertin, U. Schötzig, Coincidence summing corrections in Ge(Li)-spectrometry at low source-to-detector distances. Nucl. Instrum. Methods **158**, 471–477 (1979). https://doi.org/10.1016/S0029-554X(79)94845-6
27. L. Chen, F. Ma, X. Zhanga et al., Spallation yield of neutrons produced in thick lead target bombarded with 250 MeV protons. Nucl. Instrum. Methods Phys. Res. Sect. B **342**, 87–90 (2015). https://doi.org/10.1016/j.nimb.2014.09.020
28. Z. Zeng, Y. Mi, H. Ma et al., The characteristics of a low background germanium gamma ray spectrometer at China JinPing underground laboratory. Appl. Radiat. Isotopes **91**, 165–170 (2014). https://doi.org/10.1016/j.apradiso.2014.05.022
29. Z.K. Fan, J.L. Sun, H.X. Li et al., A novel method for simultaneous measurement of ^{222}Rn and ^{220}Rn progeny concentrations measured by an alpha spectrometer. Nucl. Sci. Tech. **36**, 8 (2025). https://doi.org/10.1007/s41365-024-01570-7
30. Y. Wang, Y.Y. Liu, B. Wu et al., Experimental investigation on the radiation background inside body counters. Nucl. Sci. Tech. **33**, 20 (2022). https://doi.org/10.1007/s41365-022-01004-2
31. G.J. Mccallum, G.E. Coote et al., Influence of source-detector distance on relative intensity and angular correlation measurements with Ge(Li) spectrometers. Nucl. Instru. and Meth. **130**, 189–197 (1975). https://doi.org/10.1016/0029-554X(75)90173-1
32. T.M. Semkow, G. Mehmood, P.P. Parekh et al., Coincidence summing in gamma-ray spectroscopy. Nucl. Instrum. Methods Phys. Res. Sect. A **290**, 437–444 (1990). https://doi.org/10.1016/0168-9002(90)90561-J
33. S. Rizzo, E. Tomarchio, Numerical expressions for the computation of coincidence-summing correction factors in γ-ray spectrometry with HPGe detectors. Appl. Radiat. Isotopes **68**, 555–560 (2010). The 7th International Topical Meeting on Industrial Radiation and Radio isotope Measurement Application(IRRMA-7). https://doi.org/10.1016/j.apradiso.2009.10.024
34. T. Vidmar, G. Kanisch, G. Vidmar, Calculation of true coincidence summing corrections for extended sources with efftran. Appl. Radiat. Isotopes **69**, 908–911 (2011). https://doi.org/10.1016/j.apradiso.2011.02.042
35. M.S. Badawi, A. Hamzawy, A.A. Thabet, Hybrid analytical method for calibrating a standard NaI(Tl) gamma-ray scintillation detector using a lateral hexagonal radioactive source. AIP Adv. **12**, 065021 (2022). https://doi.org/10.1063/5.0099399
36. Y.D. Sheng, L.Y. Song, J. Su et al., The large-scale modular bgo detection array (lambda) design and test. Nucl. Sci. Tech. **35**, 207 (2024). https://doi.org/10.1007/s41365-024-01574-3

37. L.C. He, L.J. Diao, B.H. Sun et al., Summing coincidence correction for γ-ray measurements using the HPGe detector with a low background shielding system. Nucl. Instrum. Methods Phys. Res. Sect. A **880**, 22–27 (2018). https://doi.org/10.1016/j.nima.2017.09.043
38. C. Agarwal, S. Chaudhury, A. Goswami et al., True coincidence summing corrections in point and extended sources. J. Radioanal. Nucl. Ch. **289**, 773–780 (2011). https://doi.org/10.1007/s10967-011-1126-7
39. J.M. Laborie, G. Le Petit, D. Abt et al., Monte carlo calculation of the efficiency calibration curve and coincidence-summing corrections in low-level gamma-ray spectrometry using well-type HPGe detectors. Appl. Radiat. Isotopes **53**, 57–62 (2000). https://doi.org/10.1016/S0969-8043(00)00114-7
40. A. Gupta, M. Shareef, M. Twisha et al., True coincidence summing correction for a BEGe detector in close geometry measurements. Appl. Radiat. Isotopes **200**, 110966 (2023). https://doi.org/10.1016/j.apradiso.2023.110966
41. G. Giubrone, J. Ortiz, S. Gallardo et al., Calculation of coincidence summing correction factors for an HPGe detector using GEANT4. J. Environ. Radioactiv. **158–159**, 114–118 (2016). https://doi.org/10.1016/j.jenvrad.2016.04.008
42. S. Dziri, A. Nourreddine, A. Sellam et al., Simulation approach to coincidence summing in γ-ray spectrometry. Appl. Radiat. Isotopes **70**, 1141–1144 (2012). Proceedings of the 8th International Topical Meeting on Industrial Radiation and Radioisotope Measurement Applications (IRRMA-8). https://doi.org/10.1016/j.apradiso.2011.09.014
43. D. Lijun, L. Wei, M. Jun et al., Experimental study on background reduction of γ-ray spectrometer using anticoincidence and thermal neutron shielding methods. Nucl. Tech. **33**, 501–505 (2010). https://www.hjs.sinap.ac.cn/zh/article/7235199/
44. J. Allison, K. Amako, J. Apostolakis et al., Recent developments in geant4. Nucl. Instrum. Methods Phys. Res. Sect. A **835**, 186–225 (2016). https://doi.org/10.1016/j.nima.2016.06.125
45. C. Agarwal, L. Danu, M. Gathibandhe et al., Coincidence summing corrections for a clover detector. Nucl. Instrum. Methods Phys. Res. Sect. A **763**, 240–247 (2014). https://doi.org/10.1016/j.nima.2014.06.043